

ALEGO: Towards Cost-Aware Architecture and Integration Co-Design for Chiplet-based Spatial Accelerators

Xiaochen Hao*, Zijian Ding*, Jieming Yin[†], Yuan Wang*, Yun Liang*

*Peking University

[†]Nanjing University of Posts and Telecommunications

Abstract—Advanced packaging offers a new design paradigm in the post-Moore era, where many smaller chiplets could be assembled into a large system to achieve extreme scalability and cost reduction. Recently proposed chiplet-based DNN accelerators demonstrate its effectiveness but fail to explore the tradeoffs between PPA and the fabrication cost. Specifically, we should explore both the architectural design space for individual chiplets and different integration options to assemble these chiplets. More advanced (and costly) packaging technology can enhance connectivity, but may meanwhile reduce the budget on chiplets.

In this paper, we propose ALEGO, an architecture-and-integration co-design approach for chiplet-based spatial accelerators. Based on a heterogeneous integration paradigm, ALEGO can optimize each chiplet design for different workloads to achieve better efficiency. The co-design is enabled by using uniform architecture and integration encoding and a systematic design space exploration flow. We develop an architecture modeling framework and an ML-based approach to optimize the design parameters. Experiments demonstrate that ALEGO achieves 24%, 16%, or 23% improvement in latency, energy, and cost, respectively compared with the best of separate architecture or integration optimization.

I. INTRODUCTION

The slowing of Moore’s Law has motivated the industry to embrace chiplet-based designs, where a large monolithic die is broken into multiple smaller dies called “chiplets”. Small chiplets benefit high fabrication yields and short development cycles. By leveraging advanced packaging technologies offering high-bandwidth die-to-die interconnect, designers can integrate multiple chiplets into the same package and continue delivering high-performance processors at a reasonable cost. Meanwhile, as the computing demand for machine learning keeps increasing, spatial accelerators featuring an array of processing elements (PEs) emerge as an efficient platform and also become larger and larger. For example, Cerebras [3] uses a wafer-scale accelerator to deliver cluster-scale performance. Compared with a monolithic die, chiplet-based accelerator has shown high efficiency and high scalability for machine learning workloads [6], [9], [11].

Several challenges remain in architecting the chiplets and assembling them into a package. From architectural perspective, there can be various ways to partition a monolithic chip into chiplets, and a *resource assignment* specifies the number of processing elements (PEs) and the amount of on-chip buffer in each chiplet. For spatial accelerators, *hardware dataflow* describes how a workload is parallelized and how data are moved, which determines the PE utilization and on-chip data reuse. To fully unleash performance, both resource and hardware dataflow need to be specialized for a workload.

From integration perspective, assembling multiple chiplets shows a different design angle. Partitioning a monolithic chip into chiplets requires adding die-to-die interface and thus consumes extra energy and area. The in-package wires might not deliver the same communication bandwidth and/or energy per bit as on-chip wires, thus an inefficient *in-package network* may throttle the system performance. In addition, *packaging technology* plays a pivotal role in chiplet-based designs, since it determines not only available bandwidth but also the overall fabrication cost. Depending on the performance and

budget requirement, both traditional (but cheap) and advanced (but expensive) packaging should be evaluated in the design phase.

The above architecture and integration design parameters are intertwined in a way that varying one might impact others. For example, changing the chiplet resource assignment can impact communication demands, which would subsequently affect the choice of packaging. Varying hardware dataflow can create new network hotspots, which will affect the in-package network design. To take full advantage of chiplets, we need a comprehensive chiplet-based spatial accelerator design methodology. While there exists a large body of research work on chiplet-based processors or accelerators, most of them focus on either one of the architecture or the integration aspects, and follow a separate design flow - given chiplets then design packaging [2], [13], [15], or given packaging then design chiplets [6], [9], [11]. In fact, there is a richer design space if tradeoffs can be made between the architecture and integration design. For example, we can explore the tradeoff between hardware dataflow and interconnection to improve the communication efficiency, but a separate design flow will only consider one of them at a time, leading to suboptimal design.

In this paper, we propose to *co-design* the architecture and integration of chiplet-based spatial accelerator. Specifically, the architecture design of an accelerator includes resource assignment and hardware dataflow design, while the integration of multiple accelerators includes interconnect design and packaging selection. We argue that we should consider PPPA as the design objectives, which stands for power, performance, **price**, and area, as chiplet approach can reduce cost but at the expenses of the others.

The co-design approach includes a performance modeling framework and a co-optimization framework. We target modeling an application consisting of multiple dependent DNN workloads, executed on a 3-level-hierarchy hardware consisting of a package, chiplets, and cores. The facilitated performance modeling can estimate various performance metrics for different microarchitectural designs. It models computation, data access, data reuse, and communication in a network, with a given resource assignment and mapping. The optimization framework encodes parameters from the above design aspects, and sample points from a colossal design space; each point corresponds to a unique combination of architecture and integration design, which is then evaluated using our modeling framework. We automate the design space exploration with a bayesian-based engine. The optimization can be guided by a cost-driven objective.

In summary, this paper makes the following contributions:

- We propose a co-design approach to couple architecture and integration design for chiplet-based accelerators.
- We propose a modeling framework to evaluate heterogeneous chiplet-based systems with multiple DNN workloads.
- We develop an ML-based co-optimization framework to efficiently explore the complex design space.

Experiments show that ALEGO achieves an average of 16% and 30% energy-delay-product (EDP) reduction compared with the state-

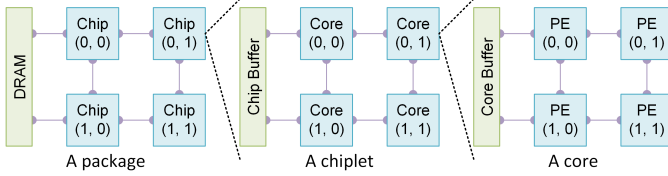


Fig. 1: A chiplet-based accelerator with distributed compute and memory units

of-the-art chiplet-based accelerators, Simba [9] and NN-Baton [11], respectively. With the co-design flow, we achieve 24% less latency, 16% less energy, or 23% less cost compared with the best of separate architecture or integration optimization.

II. BACKGROUND

A. Hardware and Application Model

We model a chiplet-based spatial accelerator in three hierarchical levels: a package, chiplets, and cores. As shown in Fig. 1, a package consists of some chiplets, and a chiplet in turn consists of multiple cores. A core has a PE array, in which every PE has a MAC unit. The operands are loaded from a DRAM, through distributed buffers in chiplets and cores, to the registers in PEs. The chiplets might be *heterogeneous* in terms of resources and dataflow. PEs, cores, and chiplets are interconnected for peer-to-peer data transfers. Multiple workloads can co-execute on different chiplets. Accordingly, the in-package network (connecting chiplets) might have routers to support arbitrary communication flow, like a network-on-chip (NoC).

We target DNN and tensor applications such as matrix multiplication, convolution, MTTKRP, etc. These workloads can be described using a loop nest, i.e., operations on tensors. We refer to *dataflow* as the way to orchestrate data movement and data reuse. The dataflow can specify where (a PE in the hierarchy) and when (a sequence) to execute a loop instance and access its associated data. The same data can be reused across interconnected PEs, or across time within the same PE. Modeling dataflow offers an accurate estimation of an accelerator's utilization, latency, and energy consumption [5], [7].

B. Advanced Packaging

Advanced packaging technologies, including organic substrate and passive/active silicon interposer, allow assembling separately manufactured dies in a package. Multiple dies are mounted on an organic substrate in Fig. 2a. A silicon interposer is a die for connectivity, as shown in Fig. 2b, on top of which dies are mounted. It interconnects dies through microbumps, which provides high interconnect density. Moreover, a passive interposer has only metal layers, while an active interposer incorporates active devices, like network routers to save bump resources. However, the passive interposer is fabricated with costly processes, while an active interposer even leverages standard CMOS processes, causing much increased costs.

We calculate the total fabrication cost of chiplet-based accelerators by considering costs of die fabrication, die bonding, substrate and interposer fabrication, and additional processes for packaging:

$$C_{total} = \sum_{i=1}^N \left(\frac{C_{die}^i}{y_{die}^i} + C_{bond} \right) + C_{sub} + \frac{C_{int}}{y_{int}} + C_{proc}$$

We consider N dies to be assembled in a package. Both die cost C_{die} and die yield y_{die} depend on the die area and technology node. The yield is estimated with a negative binomial model. The substrate cost C_{sub} and interposer cost C_{int} is also proportional to its area. The active interposer yield is estimated as a silicon die, but with the area of incorporated devices. The detailed cost is from an industrial

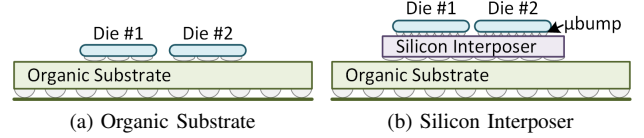


Fig. 2: Typical advanced packaging technologies.

model [1]. In this work, we focus on standard packaging technologies and fabrication costs, but our approach can be extended to industrial variants and incorporate non-recurring engineering (NRE) cost with an advanced cost model [4], [10].

III. ARCHITECTURE MODELING

In this section, we formulate the mapping problem and then present our framework and performance model.

A. Problem Formulation

Every workload defines operations on tensors and can be described using a loop nest. A mapping refers to assigning where (a chiplet), when (a sequence), and how (a dataflow) to execute these workloads:

Definition 1: Mapping. A graph $G = (V, E)$ has a set of vertices V whose element v_i is a sub-graph G' , and a set of edges E whose element (v_i, v_j) indicates v_j depends on v_i . At the lowest level, G consists of only one vertex to denote a loop instance. The mapping refers to assigning a vertex v_i onto a computing engine (PE, core, chip). The mapping has to preserve the dependence between vertices.

Fig. 3a presents an example. The input is a dependency graph of a Transformer block with two heads, which consists of five matrix multiplications (MMs, vertices 0-4). These MMs are assigned onto four chiplets, as shown in Fig. 3d. Fig. 3b shows a workload sub-graph, converted from the matrix multiply statement. Every vertex is a loop instance, and a dataflow assigns the instances to be executed on four cores (each with one PE for simplicity) at time step $t=0-2$. From a dataflow, we can analyze data reuse and its associated data communication. For example, $A[0, 0]$ is reused and forwarded from core 0 to core 1 in Fig. 3b. However, an NoC-based system needs more accurate communication modeling.

Coarse-grained Communication: The dataflow analysis implies *fine-grained communication*, where a data transfer occurs with every reuse opportunity. In contrast, a network prefers bulk data transfer in a unit of flit (e.g., 64 bytes), i.e., *coarse-grained communication*, as frequent communications cannot saturate bandwidth. Fig. 3c reflects communication with a *hierarchical dataflow*; instances are processed locally, and then the reusable data are transferred altogether. A stage at global time $gt=0$ will proceed in local time $lt=0, 1$ to process assigned instances, and then transfer $A[0, 0]$ and $A[0, 1]$ together to core 1. This approach adds a sub-graph level, with a vertex being local instances. In general, a graph hierarchy represents a hardware hierarchy; a high-level graph consists of vertices to be assigned for chiplets, and low-level graphs for cores and PEs. We could analyze data reuse and data transfer behavior at the appropriate level.

Non-uniform Communication: In an NoC-based system, communication efficiency varies with different flows, depending on network structure and traffic load. We build a communication graph with each chip being a network node to represent communication occurred with both intra-workload data reuse and inter-workload pipelining.

Definition 2: Communication Graph. A graph $G_c = (N, L)$ with each vertex $n_i \in N$ being a network node and each edge $l_{i,j} \in L$ being the communication flow from n_i to n_j , whose weight $bwr_{i,j}$ denotes its bandwidth requirement.

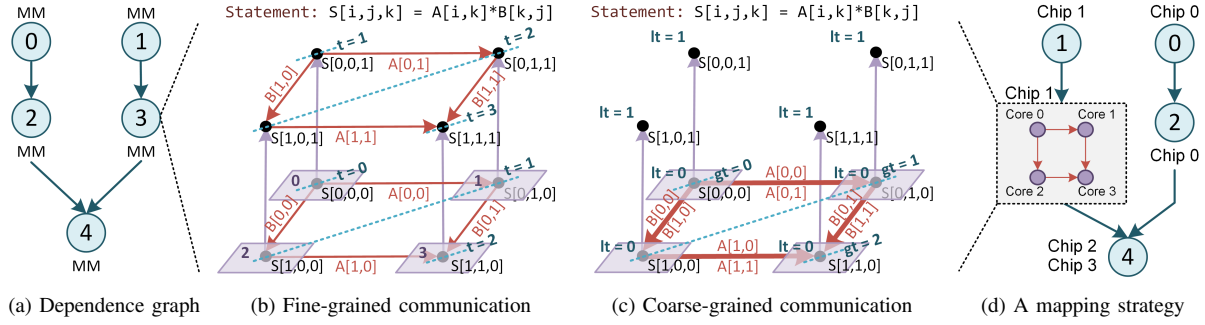


Fig. 3: The mapping formulation. The red arrows denote data transfer, and the dashed blue lines connect the instances simultaneously executed.

The communication graph can be combined with a network configuration to analyze data transfer delay. The bandwidth requirement is specific to a workload and its dataflow. Compared with the previous work [11], we propose a generic framework for multiple workloads covering various mapping schemes and microarchitectural designs.

B. Mapping framework

We first map each workload onto computing engines (PEs, cores, chips) and then analyze their dependencies. We define the computing engine domain for each workload as a cluster.

Definition 3: Cluster. A cluster is a domain of computing engines where loop instances of a workload will be mapped to. For example, the domain of chiplets in Fig. 1 is: $Chip[i, j] : 0 \leq i, j \leq 1$.

The domain of cores and PEs could be defined similarly. Every workload has its cluster exclusively, i.e., no workload is mapped to multiple clusters, and no cluster is shared between workloads. Our mapping model contains three operations. First, we associate a loop instance with a coordinate inside a cluster:

$$Map(G, \chi) = \{v \rightarrow \chi[\vec{p}_0, \vec{p}_1, \vec{p}_2]\}, \quad v \in G.V$$

where G is a workload graph, whose vertex v is a loop instance. χ is a cluster, whose element \vec{p}_{0-2} is the coordinate of chiplets, cores, and PEs, respectively. It supports various schemes, such as splitting and parallelizing a convolution along input/output channels (used in Simba [9]), or along a feature map (used in NN-Baton [11]), which exposes different parallelism and reuse opportunity. The data path is accordingly specialized, representing various microarchitectures.

Second, we associate a chiplet's coordinate inside a cluster with a chiplet in a system:

$$Bind(\chi, C) = \{\chi[\vec{p}_0] \rightarrow C[\vec{p}_0']\}$$

where C is the domain of chiplets in a system, so it binds a cluster's chiplet \vec{p}_0 to a system's chiplet \vec{p}_1 . The binding order indicates the execution sequence. For example, in Fig. 3d, we first bind workload 0 onto chiplet 0 then workload 2 onto the same chiplet, which make the two workloads executed sequentially. The cluster also provides a logical chiplet interconnects for analyzing data reuse. For example, we can bind workloads on $Chip[0, 0]$ and $Chip[1, 1]$ in Fig. 1, and the two chiplets can be considered directly connected, ignoring the real network design to build a communication graph. Then from the graph, we derive and analyze the real communication flows.

Third, we generate a hierarchical graph by reducing some vertices into a new vertex, under a specified rule:

$$Reduce_r(G, G') = \{v \rightarrow v'\}, \quad v \in G.V, v' \in G'.V$$

It reduces multiple vertices v in a graph G into a new vertex v' to generate a new graph G' under a rule r . The rule can be set to

gather instances mapped to each core, as shown in Fig. 3c. We can interleave the *map* and *reduce* operations to provide a hierarchical mapping method, i.e., assign a PE-level dataflow (*map*), gather loop instances (*reduce*), then assign a core-level dataflow (*map*), and so on. Finally, we bind the dataflow to chiplets where a workload will be executed on. These operations are performed for each workload in an application, which directs how the application is mapped.

We find that two dependent workloads could be pipelined if they are mapped to different chiplets. To make a synchronized execution of multiple workloads, we apply a *reduce* operation on the chiplet-level graph, with the rule gathering instances of a pipeline stage. For example, a batch of feature maps can be pipelined between chiplets processing different DNN layers. A reduced vertex contains computations for a batch, and can be assigned with a dataflow. However, a workload dependence graph cannot present data dependencies. For example, workload 4 is mapped to two chiplets in Fig. 3d, then we cannot find where the workload 2 and 3's results should be sent to (both the two chiplets are possible destinations). We can examine the access pattern of a tensor to build such data dependence.

Intuitively, if an element is accessed multiple times, only the first read needs external data to initialize the operation, and only the last write indicates the operations are completed. We denote the set of vertices in G that access an element $F[f]$ as $P_{G,F[f]}$, which is sorted in its execution order. A set of edges Ω represents data dependence between two workloads:

$$\Omega_{G_1, G_2} = \{(\max P_{G_1, F[f]}, \min P_{G_2, F[f]}) \mid \forall f\}$$

where G_1 and G_2 are a producer and consumer, respectively (the connected vertices in a dependence graph), and F is the dependent tensor. This equation examines each element in F , and connects the last instance (i.e., *max*) in G_1 and the first instance (*min*) in G_2 that access the same element, indicating two communicating chiplets.

C. Performance modeling

Our analytic performance model accepts a mapping description as input, and estimates different metrics considering pipeline efficiency. Multiple workloads can be pipelined (referred to as *computing stage*) and data transfer can be pipelined with computing (as *data transfer stage*). The pipeline stages can be derived by traversing the outermost mapping graph. For example, assume the whole MMs are pipelined in Fig. 3d. The workloads (e.g., MMs 0 and 2) mapped to the same chiplet are modeled as a long stage to be pipelined with others. The data transfer stages are inserted between two computing stages. The derived pipelining time diagram is shown in Fig. 4a.

We can estimate both latency and throughput. The latency refers to the delay to produce an outcome, while the throughput refers to the number of outcomes in a period. Specifically, we define a path

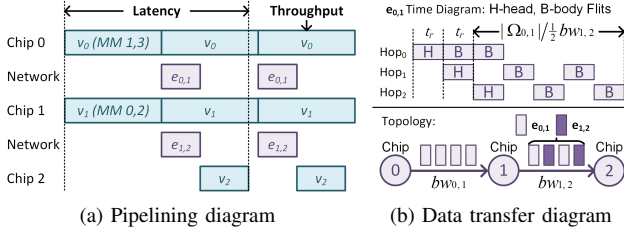


Fig. 4: Execution diagrams. $e_{0,1}$ is data transfer from chiplet 0 to 2 and $e_{1,2}$ is data transfer from chiplet 1 to 2. With a linear topology and a fair allocation policy, only half of the link bandwidth can be occupied by $e_{0,1}$.

interleaving stages $p = (v_i, e_{i,j}, v_j, \dots)$, where v_i, v_j are computing stages and $e_{i,j}$ is a data transfer stage, as shown in Fig. 4a:

$$Lat = \max_{p \in P} \left\{ \sum_{v \in p} D(v) \right\}, \quad Thr = \frac{1}{\max_{v \in V} \{D(v)\}}$$

where P is the set of paths and $D(v)$ is the delay of a stage v . The latency is the maximal sum of delays on a path, and the throughput is the reciprocal of the longest delay of all stages (in set V).

The delay of a computing stage is modeled hierarchically;

$$D_C^L = \frac{|V_L|}{U_L N} \times \max\{D_C^{LLi}, D_B^{LLi}, D_A^{LLi}\}, \quad i \in [0, N]$$

where L is a level (core or chiplet) with N lower-level (LL) engines, $|V_L|$ is the number of vertices to be mapped, and U_L is the average utilization of these engines. Every vertex's execution consumes the local processing delay, which is the maximum between computing (D_C), memory access (D_B), and data transfer (D_A) delays. These values can be obtained from a dataflow notation [5], [7].

The delay of a data transfer stage $e_{i,j}$ is preferably bounded by its associated computing stages' delay. We thus derive the bandwidth requirement as $bw_{i,j} = \frac{|\Omega_{G_i, G_j}|}{\min\{D(v_i), D(v_j)\}}$ ($|\Omega_{G_i, G_j}|$ is data transfer volume), and add it into the communication graph. From the graph, our network model estimates delays in given topology, routing, and flow control. The routing algorithm is deterministic; it always picks the same path between any two nodes. If multiple flows compete for a link (e.g., $e_{0,1}$ and $e_{1,2}$ compete for the link from chip 1 to 2 in Fig. 4b), a flow control mechanism can throttle data rate to manage resources. We can allocate bandwidth among flows in proportion to requirements if their sum exceeds the available bandwidth. The data transfer delay adds the switch and serialization delay, respectively:

$$D(e_{i,j}) = \max_{f \in F} \left\{ |f| \cdot t_s + \frac{|\Omega_{G_i, G_j}|}{\min\{ebw_c^f\}} \right\}, \quad c \in f$$

where F is the set of communication flows associated with $e_{i,j}$. $|f|$ is the hop count and t_s is the delay through one router. As shown in Fig. 4b, the head flit suffers such a delay, but the body flits are pipelined. ebw_c^f is channel c 's effective bandwidth for flow f (e.g., $ebw_{1,2}^f = \frac{1}{2}bw_{1,2}$ in Fig. 4b), and the minimum throttles a flow.

IV. OPTIMIZATION FRAMEWORK

Our proposed co-optimization framework encodes architecture and integration designs, and optimize both with an ML-based engine.

A. Co-optimization Flow

Our optimization flow encodes the involved design aspects, thus every point corresponds to a unique combination of architecture and integration design. However, there are myriad points to be explored.

We propose to separate the co-optimization flow into two stages, architecture and integration stages, as shown in Fig. 5a. The architecture stage explores chiplet designs and keeps the Pareto optimal ones. The co-design is enabled by encoding the available designs in the integration stage. We then explore the integration-related design aspects. Both stages are equipped with the ML-based optimization engine for high sample efficiency. The optimization can make trade-offs between performance, energy, cost, and area. It evaluates every sampled point using our models. The energy or area is estimated by adding overheads on MACs, memories, and networks.

B. Encoding Scheme

The architecture optimizer accepts one or more workload descriptions and explores chiplet designs where the given workloads will be mapped to. The encoding scheme we used is illustrated in Fig. 5a:

- **Shape.** The geometry of PE, core and chiplet array.
- **Spatial.** The loops that are mapped spatially. Every iteration of the loops is paralleled on a level of engines.
- **Order.** The permutation of loops indicates the execution order.
- **Tiling.** The tile size, e.g., $[I_0, J_0, K_0]$ for loops i_0, j_0, k_0 indicates a tile $A[I_0, K_0], B[K_0, J_0]$ to be processed in each chip.
- **Dataflow.** The dataflow style, e.g., 0 for the systolic array.

Every level (chiplets, cores, PEs) has a separate encoding, which is translated into mapping descriptions. Note our modeling framework covers a larger design space, including sophisticated dataflow styles (not pre-defined ones) and a non-uniform data partition (not the same tile size). The encoding strategy is designed for a single workload, but multiple workloads will be jointly optimized. We can specify the loop (e.g., a batch), inside of which would be a pipeline stage. The buffer size is adjusted accordingly to accommodate the data. Given the assignments of workloads to a chiplet, we will explore a design co-optimized for workloads mapping onto it, by fixing its resources and varying every workload's loop tiling and order.

The integration optimizer explores different package designs. The encoding scheme we used is illustrated in Fig. 5a. We give a unique number to the design alternatives (*design id*) and a unique number to all the chiplets in the selected designs (*chiplet id*).

- **Packaging.** The available options, organic substrate, passive and active interposer, are encoded as 0-2.
- **Network.** The option includes mesh and ring network.
- **Design Selector.** Each workload encodes a *design id*.
- **Technology Node.** The options from 65nm to 16nm.
- **Placement.** Each network node encodes a *chiplet id*.

The example in Fig. 5a chooses the organic substrate packaging and mesh network. Every option encapsulates an evaluation model, which accepts the designs, and outputs system-level metrics in that option, like energy, cost, or area. It chooses the 2nd and 5th designs (in the *design selector* field) to be integrated. The chiplets in the two designs are numbered; 0-1 chiplets are from the 2nd design, and 2-3 are from the 5th design. The nodes in a network are also numbered; the *placement* field $[0, 2, 3, 1]$ means putting these chiplets onto 0-3 nodes. The number of network nodes is used as a parameter. Some cases may be marked invalid in exploration; for example, the total number of chiplets exceeds that of network nodes.

We do not search network bandwidth; instead, it is derived from the bandwidth requirements. Given a communication graph and its routing, we collect the total requirements for every channel and use the maximum (i.e., a hotspot) as a bandwidth setting. The allocated I/O resource is accordingly adjusted, so different designs would lead to a large variation in some metrics like area.

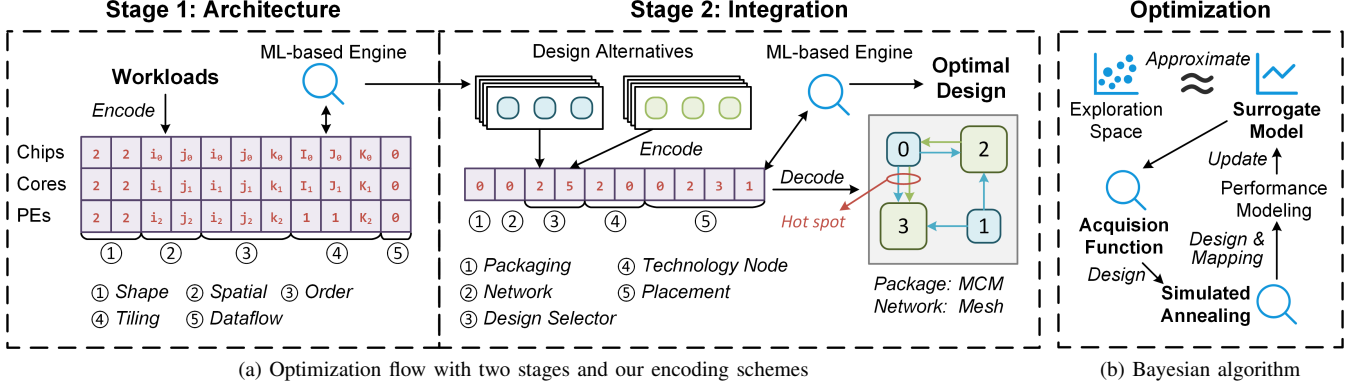


Fig. 5: The illustration of our architecture and integration co-optimization framework.

It reserves more area for data I/O in a chiplet to support higher bandwidth. A bandwidth density D_{bw} offers the allowed bandwidth per area ($GB/s/mm^2$), varying with packaging and die-to-die interface [12]. The reserved area is estimated as $\frac{b}{D_{bw}} \times N_{link}$, where b is the bandwidth, and N_{link} is the number of links through bumps. For organic substrate and passive interposer, routers are inside chiplets, so all the links pass through bumps. For active interposer, routers are inside the interposer, so only two links connected to a chiplet pass through bumps. The reserved area cannot be scaled with advanced technology and thus hinders cost reduction.

C. Optimization Engine

Our encoding scheme exposes a multi-dimensional design space that poses challenges to optimization. Though the co-optimization is separated into two stages, each stage still mingles up many parameters. We observe that a uniform encoding involves two independent phases. The architecture stage samples an accelerator **design** point, including the *shape*, *spatial*, and *dataflow* fields, then it samples a **mapping** point, including the *order* and *tiling* fields, to express how to execute a workload on that design. Similarly, the integration stage also samples a package design (*packaging*, *network*, *design selector* fields) and a mapping (*placement*, *technology node* fields) on that. Only the related fields are explored at each phase.

Fig. 5b shows our optimization engine. We use a Bayesian optimization algorithm to sample design points, then use a simulated annealing algorithm to sample mapping points. Bayesian algorithm suits an expensive black-box function; in our flow, the function is a relatively long exploration of mapping. It finds the global optimal in a few attempts, by incorporating prior information into a surrogate model. We use a *Gaussian Process* as the surrogate model, which gives the posterior distribution of an objective function and is cheap to evaluate. The acquisition function is used to select a point at each step, and we use the *probability of improvement*, which chooses a point with the highest probability better than the current optimal. A mapping point, combined with its design, is fed into our modeling framework to be evaluated in a few seconds. A simulated annealing algorithm can explore more points by leveraging randomness.

V. EVALUATION

A. Experimental Setup and Validation

We use TENET [7] for data reuse analysis, and Accelergy [14] for area and energy modeling. The fabrication cost is from an industrial model [1]. The die-to-die interface setting is UCIE [12]. We validate the proposed modeling framework against ScaleSim [8], a systolic array simulator. We set a four-chip accelerator running Transformer,

in which each chip has an 8×8 PE array. The latency estimated by ALEGO is within 9.8% error against the simulation results.

B. Comparison

We compare ALEGO against state-of-the-art chiplet-based DNN accelerators, i.e., Simba [9] and NN-Baton [11], by realizing their hardware configurations and mapping strategies in our framework. We collect workloads from typical NN models, *res[2-5]* *b_branch2b* convolution layers from Resnet-50, and four matrix multiply shapes from BERT-large. The parameters are searched with our optimizer.

We use energy-delay product (EDP) as the optimization objective. Fig. 6 shows an energy and latency comparison, as well as an energy breakdown. Results are normalized to that of Simba in every setting. We achieve an average of 16% and 30% EDP reduction compared with Simba and NN-Baton, respectively.

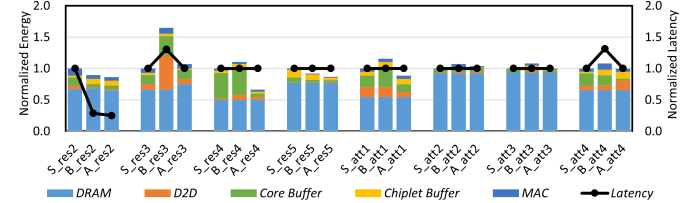


Fig. 6: The optimization results. We label each group with a prefix (S for Simba [9], B for NN-Baton [11], and A for ALEGO), then the workload name: *res[2-5]* are from ResNet-50, and *att[1-4]* are from BERT-large.

We achieve an average of 8% and 20.8% energy reduction compared with Simba [9] and NN-Baton [11], respectively. NN-Baton uses a ring network where data are rotated among chiplets. It picks the input with less volume to be reused. For example, in activation-intensive layers (with large feature maps), it reuses weights among chiplets. This strategy gains benefits in settings with unbalanced data volume, such as *res2*, to transfer fewer data and show lower energy than Simba. However, significant die-to-die data transfer overhead is observed when two inputs are both large, such as *res3*. For latency comparison, Simba maps loop instances by dividing input and output channels so that it might suffer a longer latency on the earlier layer (e.g., *res2*) with insufficient parallelism on channels. NN-Baton maps instances by dividing the output plane and thus performs worse with insufficient parallelism on outputs.

In summary, different workloads have their preferred microarchitecture design. We leverage the heterogeneous integration paradigm to optimize a design for a specific workload, and propose a generic framework to cover various design options.

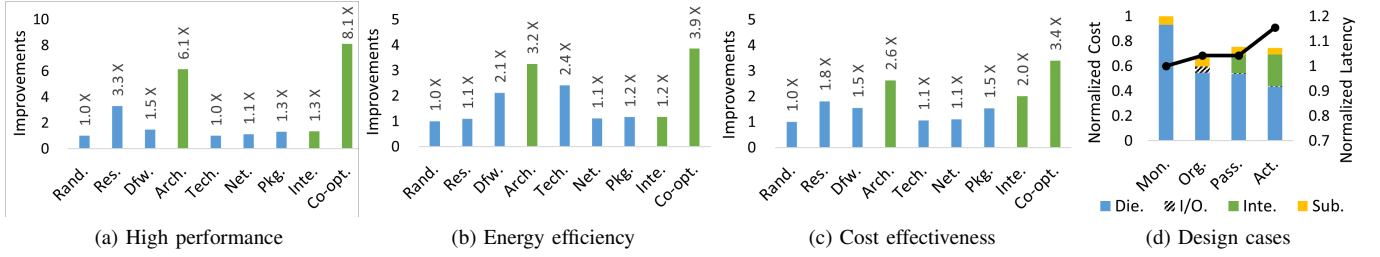


Fig. 7: The design space analysis. In figure (a)-(c), we label each setting as follows: *Rand*: Random, *Res*: Resource, *Dfw*: Dataflow, *Arch*: Architecture, *Tech*: Technology Node, *Net*: Network, *Pkg*: Packaging, *Inte*: Integration, *Co-opt*: Co-optimization. In figure (d), we label each setting as *Mon*: Monolithic Die, *Org*: Organic Substrate, *Pass*: Passive Interposer, *Act*: Active Interposer. *Inte* and *Sub* refers to the interposer and substrate cost, respectively.

C. Design Space Analysis

The proposed co-design approach shows a colossal design space. We separately enable different optimizations and their combinations to demonstrate the co-design efficiency. We evaluate a Transformer block by mapping every workload to different chiplets. We set three optimization objectives, high performance, energy efficiency, and cost effectiveness, to evaluate the impact of every design aspect. We set the baseline as a *random* setting, which has a Simba-like hardware configuration, while other parameters are randomly sampled. The relative improvements by enabling different optimizations are reported in Fig. 7a-7c, for the three objectives respectively. We achieve 24% less latency, 16% less energy, or 23% less cost compared with the best of separate architecture or integration optimization.

We set the performance metric as *latency*, and report the latency reduction in Fig. 7a. The architecture optimization (4th bar), combining resource assignment and dataflow, leads to a high 6.1 \times latency reduction with more PEs and improved utilization. The integration optimization (8th bar), coordinating technology, network, and packaging, leads to 1.3 \times latency reduction. As discussed in § IV-B, our bandwidth setting varies with the hotspot. Varying network changes interconnect designs and node placements, while varying packaging changes chiplets to be integrated, thus incur new hotspot and affect its bandwidth allocation. Overall, co-optimizing computing and data communication shows an 8.1 \times reduction (9th bar).

The results for energy optimization are presented in Fig. 7b. The architecture optimization can achieve 3.2 \times energy reduction, where different design aspects interact mutually. Allocating a larger buffer would consume more energy, but also benefits dataflow optimization that leverages on-chip data reuse and reduces off-chip memory accesses. The integration optimization leads to 1.2 \times energy reduction. Though varying technology scales down almost all energy overhead, it is from an ideal scaling factor, and may cause unfair comparisons with others. We disable changing technology nodes when reporting the related results (8th and 9th bar in the figure). Varying network and packaging can reduce the overhead on die-to-die interface, and benefit from advanced packaging (0.25pJ/bit vs. 0.5pJ/bit [12]).

We introduce a new metric to characterize cost effectiveness, the product of cost and log-normalized EDP, referred to as *scaled cost* (lower is better). The normalized EDP can penalize designs with high energy or high latency. We report the cost reduction in Fig. 7c. The architecture optimization achieves a 2.6 \times cost reduction, owing to smaller die (by varying resources) and smaller network (by varying dataflow to reduce inter-chiplet data transfer). The integration optimization leads to 2.0 \times cost reduction. Though making chips smaller, advanced technology node has minor improvement; manufacturing a chip becomes more costly, and the reserved area for data I/O cannot be scaled. Varying network and packaging results in a more efficient interconnect design and thus reduces the cost for data I/O.

D. Design Cases

The co-design space facilitates comprehensive tradeoffs. Fig. 7d shows four Pareto optimal designs for a VGG-16 model, regarding latency and cost, with a given packaging option. We assemble four chiplets with organic substrate or passive/active interposer, and set a monolithic die as the baseline. The area constraint of all chiplets (or a monolithic die) is 400mm² (28nm), on par with a TPU chip. We can observe a significant die cost reduction in chiplet-based designs, as small dies enjoy better yields. I/O cost, a part of the die cost for inter-chiplet communication, shrinks with more advanced packaging technologies. However, the interposer is costly; nearly 20% of the cost pay on this. A tradeoff can be made between cost and latency; for active interposer (4th bar in Fig. 7d), a smaller die is picked to amortize the interposer cost, making higher latency.

VI. CONCLUSION

In this paper, we propose ALEGO, a co-design framework for chiplet-based accelerators that couples architecture and integration designs. It facilitates a comprehensive tradeoff between architecture and integration designs, and incorporates fabrication costs to guide optimization. Our proposed modeling framework expands the design space, and our proposed optimization flow offers 24% less latency, 16% less energy, or 23% less cost compared with the best of separate architecture or integration optimization.

REFERENCES

- [1] "IC Knowledge cost models," <https://www.icknowledge.com/>.
- [2] S. Bharadwaj *et al.*, "Kite: A family of heterogeneous interposer topologies enabled via accurate interconnect modeling," in *DAC*, 2020.
- [3] Cerebras, "The Future of AI is Here," <https://cerebras.net/chip/>.
- [4] Y. Feng *et al.*, "Chiplet actuary: A quantitative cost model and multi-chiplet architecture exploration," in *DAC*, 2022.
- [5] H. Kwon *et al.*, "Understanding reuse, performance, and hardware cost of dnn dataflow: A data-centric approach," in *MICRO*, 2019.
- [6] Y. Li *et al.*, "Scaling deep-learning inference with chiplet-based architecture and photonic interconnects," in *DAC*, 2021.
- [7] L. Lu *et al.*, "TENET: A framework for modeling tensor dataflow based on relation-centric notation," in *ISCA*, 2021.
- [8] A. Samajdar *et al.*, "A systematic methodology for characterizing scalability of dnn accelerators using SCALE-sim," in *ISPASS*, 2020.
- [9] Y. S. Shao *et al.*, "Simba: Scaling deep-learning inference with multi-chip-module-based architecture," in *MICRO*, 2019.
- [10] D. Stow *et al.*, "Cost-effective design of scalable high-performance systems using active and passive interposers," in *ICCAD*, 2017.
- [11] Z. Tan *et al.*, "NN-Baton: DNN workload orchestration and chiplet granularity exploration for multichip accelerators," in *ISCA*, 2021.
- [12] UCle, "UCle white paper," <https://www.uciexpress.org/general-8>.
- [13] M. Wang *et al.*, "Network-on-interposer design for agile neural-network processor chip customization," in *DAC*, 2021.
- [14] Y. N. Wu *et al.*, "Accelergy: An architecture-level energy estimation methodology for accelerator designs," in *ICCAD*, 2019.
- [15] J. Yin *et al.*, "Modular routing design for chiplet-based systems," in *ISCA*, 2018.